NMR Measurements and Numerical Simulation of Fluid Transport in Porous Solids

J. J. Tessier and K. J. Packer
Dept. of Chemistry, University of Nottingham, Nottingham NG7 2RD, U.K.

J.-F. Thovert
LPTM, SP2MI, BP 179, 86960 Futuroscope Cedex, France

P. M. Adler
IPGP, 75252 Paris Cedex 05, France

Pulsed magnetic field gradient stimulated echo NMR measurements are performed for diffusion and flow of an aqueous phase both within a sample of packed spherical beads and within a 25% porosity Fontainebleau sandstone. The stimulated echo dependence on the gradient pulse area q is used to derive the displacement probability distributions $P_\Delta(X)$ for fixed observation times Δ. The shape of $P_\Delta(X)$ as a function of Δ is simulated for computer-generated porous media, and a good agreement is obtained between the experimental NMR data and the simulations.

Introduction

The experimental study of fluid transport has made substantial progress in recent years with the use of techniques such as laser velocimetry (Cenedese and Viotti, 1996; Durst et al., 1981; Saleh et al., 1996). Unfortunately, there remains a large class of systems for which such existing methods are difficult to employ. This is particularly the case for optically opaque materials such as many porous solid media. For these materials, nuclear magnetic resonance (NMR) and microtomography (Spanne et al., 1994; Auzerais et al., 1996) offer convenient means to study fluid transport. In this article, we describe the use of pulsed magnetic field gradient spin-echo (PGSE) NMR methods to characterize molecular displacements in both a random loose packing of spherical grains and in a 25% porosity Fontainebleau sandstone (permeability: 2.05 *D*) in which the fluid transport arises from both self-diffusion and externally-driven flow.

While considerable attention has been given to the characterization of self-diffusion by the PGSE NMR techniques, the few NMR studies of flow in porous materials have until recently used either time-of-flight methods or have focused on the measurement of average flow velocity. To our knowledge, a complete analysis of fluid transport in porous media has not yet been presented in the context of NMR, although initial steps in this direction have recently been reported (Seymour and Callaghan, 1996; Lebon et al., 1996; Packer and Tessier, 1996; Kutsovsky et al., 1996). In the work presented here, the molecular displacement distributions obtained by NMR are compared with computer simulations based on techniques described in detail by Adler et al. (1990) and summarized below.

Experimental Studies

The NMR measurements were performed using a GE Omega CSI spectrometer provided with a 2T 310-mm-ID horizontal bore magnet and a set of S-150 Accustar actively-shielded 150 mm inner diameter gradients coils, generating gradients of up to 0.2 $T \cdot m^{-1}$. In this study, the NMR sequence (APGSTE) shown in Figure 1 was used to minimize the effects of molecular displacements through the internal magnetic field gradients, which arise from the differences of magnetic susceptibility existing between the porous solid matrix and the saturating fluid (Lucas et al., 1993). The NMR procedure for motion encoding used here is intended to be robust rather than optimal in terms of time efficiency. In particular, the phase of each radio-frequency pulse in the NMR sequence was fully cycled to remove unwanted signals. This phase cycling was adapted from Fordham et al. (1994) to discriminate the effects of positive and negative displacements on the NMR signal. This is done by offsetting the phase of the second 90° pulse by $\pi/2$ to measure both transverse components of the NMR stimulated echo signal.

When the applied gradient pulses are sufficiently narrow that we can neglect motion over their duration ($\delta \ll \Delta$), the response of the APGSTE NMR sequence can be written as

$$S_\Delta(q_x) = S_o \int P_\Delta(X) \exp(2\pi i q_x X) dX \qquad (1)$$

Correspondence concerning this article should be addressed to K. J. Packer.

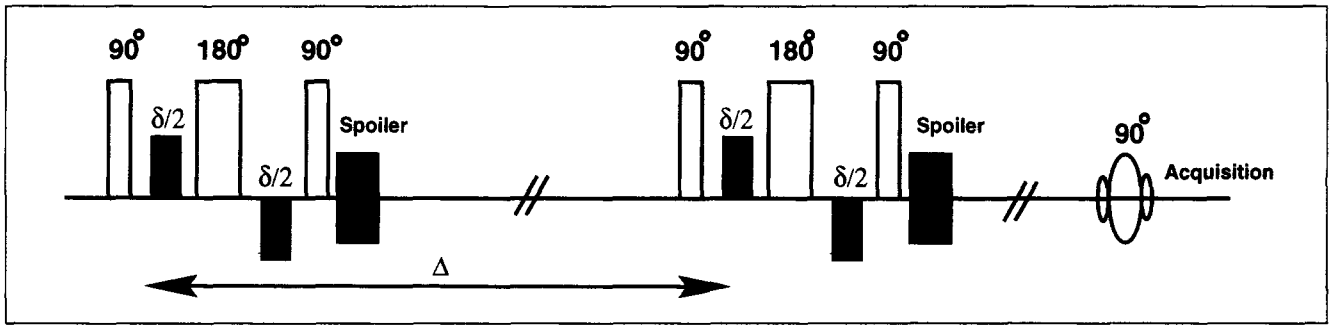

Figure 1. Pulsed gradient stimulated echo NMR sequence used for the measurements of fluid transport in porous solid.

r.f. pulses are gray; gradient pulses are black.

with

$$P_\Delta(X) = \int P(x_o)P(x,\Delta;x_o)dx_o \qquad (2)$$

where the displacement $X = x - x_o$ and $P(x_o)$, $P(x,\Delta;x_o)$ are respectively the probability density for starting positions and the probability for displacement from x_o to x in a time Δ (Callaghan, 1991). The direction X is defined by the direction of the magnetic field gradient while the area of the gradient pulses is accounted for by $q_x = \gamma\delta g_x/2\pi$. Equation 1 implies that the so-called average propagator (probability density) $P_\Delta(X)$ for fluid displacement is obtained by measuring the NMR signal $S_\Delta(q_x)$ and Fourier transforming with respect to q_x. In this article we present measurements of $P_\Delta(X)$ as a function of the observation times Δ for the transport of a single-phase fluid in two porous media.

Flow through a bed of spherical beads

In these experiments, water was flowed at 57mL/min in a 5-cm-ID cylindrical perspex tube packed with 3-mm-dia. glass beads. For glass beads of this diameter, the relaxation and susceptible characteristics of the sample are such that NMR can be used to obtain accurate porosity measurement. The porosity of the sample of packed beads ($\epsilon = 0.44$) was measured by comparing the intensity of the NMR signal obtained on the porous medium with the NMR signal measured on samples of known porosities. The water flow was controlled by a constant head pressure arrangement. The NMR signal was obtained for a selected axial slice of thickness 40 mm, using 32 or 64 q_x values in the range $\pm q_{max}$. q_{max} and the number of q values were adjusted to capture the displacement of the molecules correctly and to avoid truncation of the NMR signal $S_\Delta(q)$ at $\pm q_{max}$. The observation time Δ was varied from 63 to 2,010 ms to maintain a good approximation for the narrow pulse condition ($\delta \ll \Delta$) and an acceptable signal-to-noise ratio. The gradient pulse width δ was typically set to 6 ms. The NMR data were transferred to Unix SUN Sparc workstations for processing, interpolation, and display. Prior to Fourier transformation, the NMR signals $S_\Delta(q_x)$ were zero filled to 256 points. The $P_\Delta(X)$ distributions were phased and subsequently normalized by dividing by $\int P_\Delta(X)\,dX$ in each case.

Flow in Fontainebleau sandstone

The sample was a cylinder of Fontainebleau sandstone (porosity = 25%, permeability = 2.05 D), 39 mm in diameter and 52 mm in length. This was fully saturated with a 3% w/v aqueous NaCl solution and was contained in a specially constructed sample holder which provided a hydrostatic pressure (28 bar) around the cylindrical surface of the sandstone through a close-fitting sleeve pressurized on the outside with Fluorinert FC 16001. This prevents bulk radial flow and any flow of fluid around the perimeter of the core. The brine flow in the axial direction was driven by a precision pump (Pharmacia P 500) at a fixed flow rate of 400 mL/h. The NMR signal $S_\Delta(q)$ was obtained by selecting a slice of thickness 40 mm and by using up to 128 values of q_x. The gradient pulse width δ was typically set to 6 ms.

Modeling

The determination of the probability $P_\Delta(X)$ necessitates three steps. First, an adequate representation of the porous medium must be simulated; this has been done by using two techniques: sphere packings (Coelho et al., 1996) and reconstructed media (Adler et al., 1990). Second, the local flow field is determined in the pores of the medium by solving the Stokes equations. Third, the fluid is seeded with a large number of particles which undergo convection and Brownian diffusion; the knowledge of the positions of these particles after a time Δ enables us to calculate the previous probability distribution $P_\Delta(X)$ defined by Eq. 2.

Reconstruction of porous media

Two entirely different types of media have been used in the experiments, and they are reconstructed by two different techniques. Random packings of spheres result from the successive deposition of grains in a "gravitational" field; a general algorithm valid for particles of any shape has been devised by Coelho et al. (1996), which can be easily specialized to spherical particles. The grains are introduced at a random location above the bed already in place, and fall until they reach a local minimum of their potential energy. During their fall, any displacement and rotation which contribute to lower their barycenter are allowed. Note that a simplified point of view was adopted, which is mostly based on a kinematic and

steric analysis; hence, the various forces which may act on a particle in a real experiment are not taken into account.

As a general rule, a mobile particle is allowed to slip freely on the bed surface as long as the elevation of the barycenter can be diminished. Moreover, each elementary displacement of a grain is independent of its previous position and orientation increments. However, an adjustable parameter allows to favor either translation or rotation of the particle, when both motions could lower its elevation. The interactions are reduced to steric exclusion. A variant of this rule has been devised to simulate short-range attractive forces, which could create permanent links between grains. After contact, a settling grain can be allowed to rotate around the contact point without a slip (but the contact may move if the grain rolls on the bed). Generally speaking, periodicity conditions are imposed along the two horizontal axes in order to be consistent with the flow calculations.

This general algorithm can be simplified when spheres are considered. The minimal porosity which could be obtained for a particular choice of the construction parameters (Coelho et al., 1996) is equal to 0.402, which is in good agreement with the standard literature data.

In order to simulate the experiments, a random packing of monodisperse spheres was constructed numerically by this technique with periodicity conditions along the two horizontal axes. The sample is made of N_C^3 elementary cubes of size a = 300 μm, with $N_C = 64$. By choosing the construction parameters, the porosity was adjusted to the experimental value $\epsilon = 0.44$. The grain diameter is approximately equal to 10 elementary cubes. The bed permeability K was calculated by solving the Stokes equations. It was found that $K = 7{,}140$ Darcy. An example of such a packing is displayed in Figure 2.

The second type of porous medium which has been used in these experiments is Fontainebleau sandstone. Let us briefly summarize the reconstruction process which has been devised (Adler et al., 1990) and applied here. The statistical properties of the medium are measured on thin sections. The phase function $Z(\boldsymbol{x})$ is introduced

$$Z(\boldsymbol{x}) = 1 \quad \text{if x belongs to the pore space} \qquad (3)$$
$$= 0 \quad \text{otherwise}$$

where $\boldsymbol{x}$ denotes the position with respect to an arbitrary origin.

The porosity ϵ and the correlation $R_z(\boldsymbol{u})$ can be defined by the statistical averages (which will be denoted by an overbar)

$$\epsilon = \overline{Z(\boldsymbol{x})} \qquad (4)$$

$$R_Z(\boldsymbol{x}) = \frac{\overline{[Z(\boldsymbol{x}) - \epsilon][Z(\boldsymbol{x}+\boldsymbol{u}) - \epsilon]}}{\overline{[Z(\boldsymbol{x}) - \epsilon]^2}} \qquad (5)$$

The generation of an homogeneous and isotropic medium with a given porosity ϵ and a given correlation function is equivalent to the generation of a random function of space $Z(\boldsymbol{x})$ which is equal to 0 in the solid phase and to 1 in the liquid phase, and such that it satisfies the two average properties (Eqs. 4 and 5). For practical purposes only, the porous medium is constructed in a discrete manner.

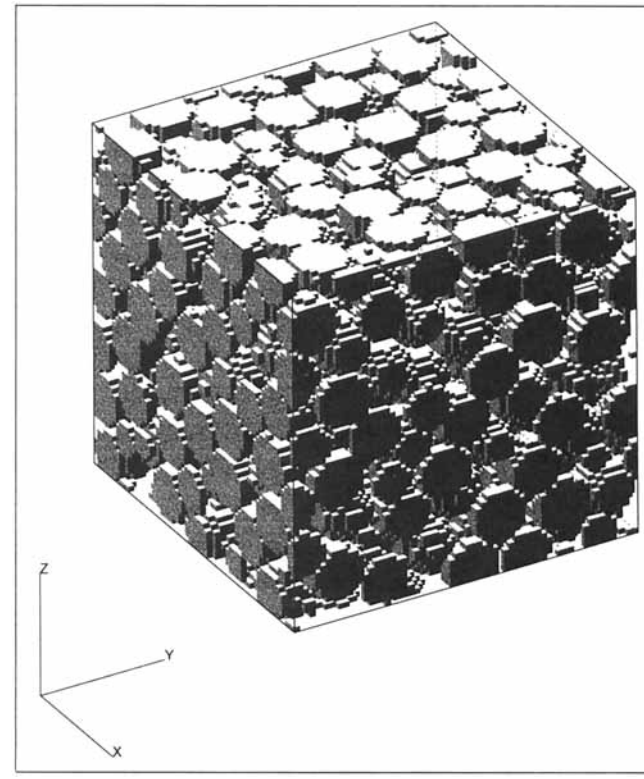

Figure 2. Example of reconstructed packed bed of monodisperse spheres.

It is considered as being composed of N_C^3 small cubes of side a. These elementary cubes are filled either with liquid or with solid.

The reconstruction of the porous medium will only be briefly sketched since a detailed presentation can be found in Adler et al. (1990) and Adler (1992). The principle is similar to the algorithms due to Joshi (1974) and Quiblier (1984) for two- and three-dimensional media, respectively. Technical differences exist such as the replacement of the linear combinations of independent Gaussian variables by an explicit method based on the use of Fourier transforms; this modification improved considerably the numerical efficiency of the process. Another important difference is the use of periodic boundary conditions during the generation of the samples; these condition are consistent with the analysis of the flow properties as will be seen next.

The generation process consists of two major steps. A Gaussian and uncorrelated field $X(\boldsymbol{x})$ can be generated at the center of each elementary cube. A Gaussian field $Y(\boldsymbol{x})$ with a given correlation function $R_Y(\boldsymbol{u})$ can be derived from $X(\boldsymbol{x})$ by Fourier transform techniques. Finally, a discrete field $Z(\boldsymbol{x})$ can be obtained by application of the following nonlinear filter

$$Z(\boldsymbol{x}) = 0 \quad \text{if } Y(\boldsymbol{x}) \le a(\epsilon) \qquad (6)$$
$$Z(\boldsymbol{x}) = 1 \quad \text{if } Y(\boldsymbol{x}) > a(\epsilon)$$

For Gaussian distributions, the threshold $a(\epsilon)$ is easily determined. Moreover, the correlation $R_Z(\boldsymbol{u})$ of the variables

$Z(x)$ (Eq. 5) must be related to the correlation $R_Y(u)$ of the variables Y by

$$R_Z(u) = \mathfrak{F}_\epsilon[\,\mathfrak{R}_y(u)] \tag{7}$$

where $\mathfrak{F}$ is a function which depends upon ϵ and which is expanded as a series.

Hence, when one wants to simulate a porous medium, the first step consists of the inversion of Eq. 7 to obtain $R_Y(u)$. This can be performed by any standard Newton iterative scheme. The Fourier transform of $R_Y(u)$ is also obtained numerically.

Once the Fourier transform of $R_Y(u)$ is known, arbitrary samples of porous media can be reconstructed. One starts from an arbitrary seed and generates a set of independent Gaussian variables $X(x)$ for each elementary cube; then this set is successively correlated and thresholded in order to obtain the variables $Y(x)$ and $Z(x)$.

It is useful to give in Figure 3 an example of a three-dimensional reconstructed medium; the apparent realism of this piece of material is quite striking. It should be emphasized that no additional parameter is needed to generate this medium.

Determination of the flow field

The following algorithm applies whatever the structure of the porous medium being studied.

Once finite samples of porous media are generated, the flow field of Newtonian fluids at low Reynolds number can be determined (Lemaitre and Adler, 1990). The low Reynolds number flow of an incompressible Newtonian fluid is governed inside a unit cell of size N_C by the usual Stokes equations

$$\nabla p = \mu \nabla^2 v, \quad \nabla \cdot v = 0 \tag{8}$$

where v, p and μ are the velocity, pressure, and viscosity of the fluid, respectively. In general, v satisfies the conditions

$$v = 0 \quad \text{on } S, v \text{ is spatially periodic} \tag{9}$$

S denotes the surface of the wetted solid inside the unit cell. This system of equations and the conditions apply locally at each point R of the interstitial fluid. In addition, it is assumed that the macroscopic pressure gradient ∇p is specified

$$\overline{\nabla p} = \text{a prescribed constant vector} \tag{10}$$

The seepage velocity $\bar{v}$ is related to $\overline{\nabla p}$ by the permeability tensor K such that

$$\bar{v} = -\frac{1}{\mu} K \cdot \overline{\nabla p} \tag{11}$$

Here K is a symmetric tensor that is positive definite. It only depends on the geometry of the system and thus can be simplified when the porous medium possesses geometric symmetries. For isotropic materials, K is a spherical tensor, that is, $K = KI$, where I is the unit tensor.

The numerical method to solve these equations is described by Lemaitre and Adler (1990). This methodology was first evaluated by Adler et al. (1990) on Fontainebleau sandstones.

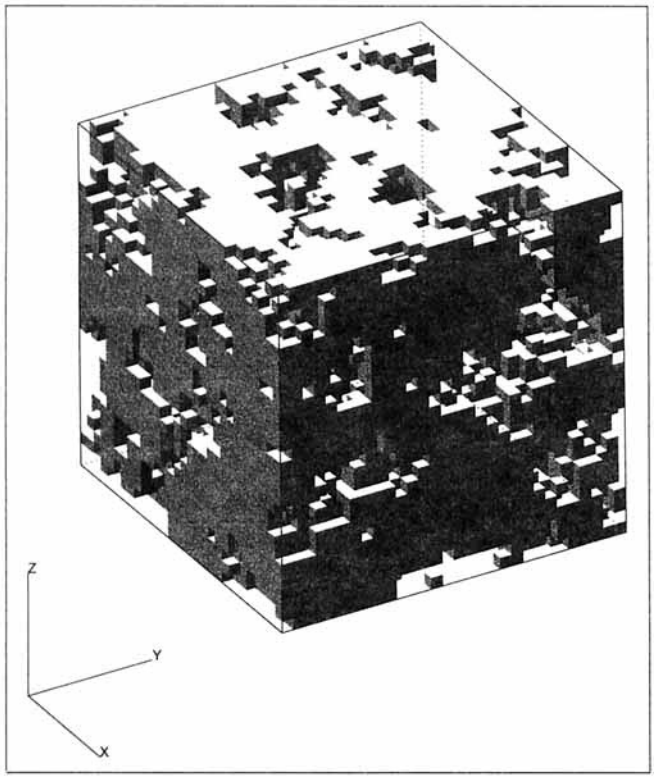

Figure 3. Example of reconstructed medium based on a Fontainebleau sandstone.

Dispersion of particles

In order to determine the probability $P_\Delta(X)$ (Eq. 2), the simplest technique consists of calculating the individual trajectories of convected Brownian particles. This method has already been applied a number of times, for instance, for the determination of the macroscopic dispersion tensor (Salles et al., 1993). First, the velocity field is determined as before. Then, at time zero, a large number N_P of particles is released in the pore space. The initial distribution of particles is uniform in the pore space.

During all subsequent elementary time steps δt, the position of each particle i is updated by adding a convective displacement and a random diffusive one

$$r_i(t + \delta t) = r_i(t) + \delta_i \tag{12}$$

$$\delta_i = v(r_i)\delta t + \delta_D \tag{13}$$

Whenever $r_i(t) + \delta_i$ falls within the solid, the particle stops at the solid wall and its clock is incremented by a fraction of δt

$$r_i(t + \lambda \delta t) = r_i(t) + \lambda \delta_i, \quad 0 \le \lambda \le 1 \tag{14}$$

At subsequent time steps, the particle starts from this location. Since particles close to the walls may accumulate time delays, at regular time intervals these delayed particles are allowed to catch up with time.

The direction of the random jump δ_D is chosen randomly. Except when wall collisions occur, its magnitude δ_D is constant and related to the molecular diffusivity D.

$$\delta_D^2 = 6D\delta t \tag{15}$$

When the Stokes equations are solved, the velocity field v is only known at the grid points with a fourth-order error. The velocity $v(r_i)$ is obtained everywhere by a second order Taylor expansion. The dimensionless parameter which compares convective and diffusive effects is the Peclet number

$$Pe = \frac{\overline{v^*}L}{D} \tag{16}$$

where $\overline{v^*}$ is the interstitial velocity and L is a characteristic length. L is equal to the sphere diameters for the sphere packings and to the correlation length of the porous medium for the Fontainebleau sandstones.

In order to keep the elementary jump δ_i reasonably small, δt and the flow rate are adjusted for a given Peclet number so that δ_D is as large as possible (which speeds up the statistical convergence) while maintaining

$$|\delta_i| < \delta_M \tag{17}$$

where δ_M is the maximal value of the elementary jump; this value is smaller than $a/2$, where a is the size of the elementary cubes.

Thus, it is possible to follow the evolution of the particles with time.

Summary of calculations

The computations can be run as follows. Sphere packings and the Fontainebleau sandstone are reconstructed. Then, the velocity field is determined in the sample within a multiplicative constant by integrating the Stokes equations. A large population of N particles is distributed at random within the pore space at time t. A random walk is performed until time $t + \Delta$ by adding successive random and deterministic elementary displacements, which simulate the convection-diffusion process. When the positions of all the particles are determined at time $t + \Delta$, the so-called average propagator $P_\Delta(X)$ is calculated. According to Eq. 2 and with the same notations, $P_\Delta(X)\,dX$ is the proportion of particles which undergo a displacement ranging from $X - dX/2$ to $X = X + dX/2$.

$$P_\Delta(X)dx = dX\int P(x_o)P(x,\Delta;x_o)dx_o \tag{18}$$

$$= N^{-1}\Big(\text{number of particles } i/x_i - x_{io} \in \Big[x - x_o - \frac{dx}{2}, x - x_o + \frac{dx}{2}\Big]\Big)$$

The displacement X can be chosen along any direction. In practice, it is taken either along the main direction of the flow or perpendicular to it; the corresponding average propagator $P_\Delta(X)$ is then denoted $P_\Delta\|$ and $P_\Delta\perp$, respectively.

Results and Discussion

Random loose packings of spheres

Bead packings were investigated both numerically and experimentally. In the real bed, the sphere diameter is 3 mm and the porosity $\epsilon = 0.44$. NMR measurements were performed without flow or with a flow with a mean interstitial velocity 1.1 mm/s over a 2-s time range. Three features should be mentioned here. First, the Peclet number of the flow is very large

$$Pe = \frac{\overline{v^*}L}{D} = 1{,}570 \tag{19}$$

where the length scale L is the bead diameter. Second, the Reynolds number Re, which is defined as the ratio of inertial and viscous forces is greater than unity

$$Re = \frac{\overline{v^*}L}{\upsilon} = 3 \tag{20}$$

where υ is the kinematic viscosity of the fluid.

Third, the NMR experiments correspond only to a very short initial transient of the dispersion process. The root-mean-square diffusive displacement of the molecules during 1 s ($\sqrt{2DT} = 65\ \mu$m) is much smaller than the grain size. Therefore, in the absence of flow, the geometry of the medium has little influence and the propagator should spread like that of an unconfined fluid. This feature is accurately verified in the NMR experiments with a self-diffusion coefficient $D = 2.1\times10^{-9}\text{m}^2\cdot\text{s}^{-1}$, obtained from the NMR APGSTE experiment (Figure 1). In the presence of flow and for displacements measured along the average flow direction (Figure 4), the $P_\Delta(X)$ distributions corresponding to an aver-

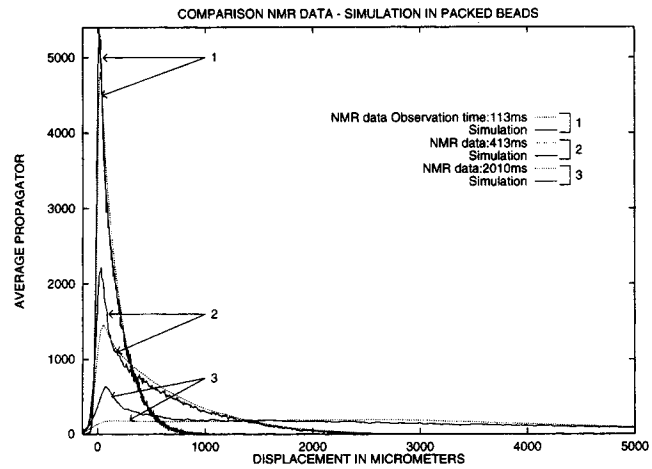

Figure 4. $P_\Delta(X)$ for water flow ($Q_w = 57$ mL/min) in packed beads.

Measurements and simulations made along the flow direction.

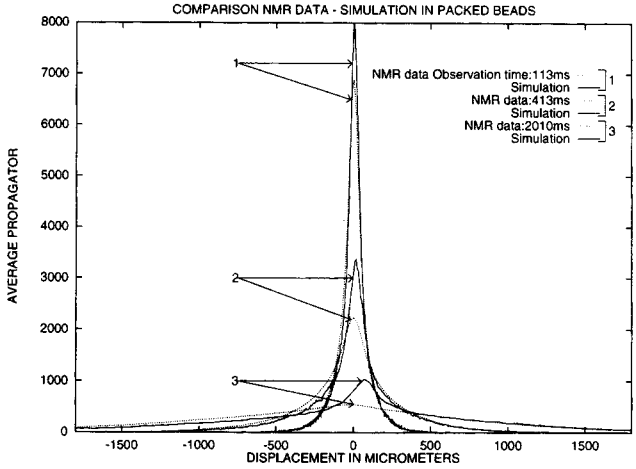

Figure 5. $P_\Delta(X)$ for water flow ($Q_w = 57$ mL/min) in packed beads.

Measurements and simulations made perpendicular to the flow direction.

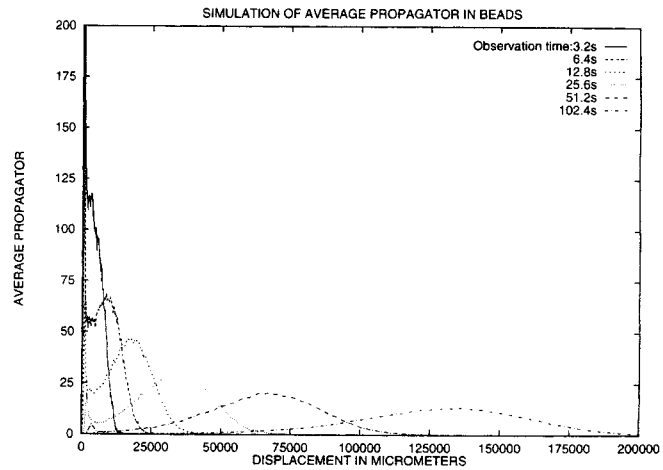

Figure 6. Simulated average propagator $P_\Delta(X)$ in a random bead packing of porosity $\epsilon = 0.44$ parallel to a flow with a mean interstitial velocity $v^* = 1.1$ mm/s.

Numerical simulations for long observation times Δ.

age displacement $\langle X \rangle < 500$ μm are strongly peaked close to zero, are asymmetric in the direction of the flow, and increase their spread in this direction as Δ is increased. At longer times for which $\langle X \rangle > 500$ μm, the $P_\Delta(X)$ increasingly shows an evolution to a more Gaussian-like shape. The distributions for displacement perpendicular to the average flow direction (Figure 5) are symmetric with respect to zero displacement, as would be expected, because of the constraint of zero net flow in this direction.

The results of the simulations are plotted in Figures 4 and 5 in comparison with the experimental data. The bed permeability K was calculated by solving the Stokes equations. It was found that $K = 7{,}140$ Darcy. Consider first the direction parallel to the flow (Figure 4). A good agreement is observed for small times. Then, for $t \geq 400$ ms, the peak at zero-displacement decreases more slowly in the simulations than in the NMR experiments although the agreement for the rest of the curves, that is, for large displacements, remains good. For longer times, the experimental and numerical curves differ mainly by the height of the peak near the origin. For completeness, the simulation results over longer times (up to 100 s) are presented in Figure 6. It takes about 50 s to completely erase the peak near zero displacement. Note that during this time, the rms diffusive displacement of the particle is still much smaller than the bead diameter (less than 500 μm).

Similar conclusions can be drawn from Figure 5 for the direction normal to the flow. A good overall agreement is obtained at early times (100 ms). Later, the agreement is good except for the peak at zero displacement.

This permanent feature may be due, partly or totally, to the very large value of the Peclet number (Eq. 19). It was shown in earlier works (Salles et al., 1993) that random walk simulations become very sensitive to small inaccuracies in the computation of the velocity field when $Pe \geq 1{,}000$. Note, however, that the dispersivity coefficients determined from the long-time simulations of Figures 4 and 5 ($D^*_{\parallel}/D = 3{,}000$, $D^*_{\perp}/D = 80$) are in very good agreement with literature data (Coelho et al., 1996). As mentioned earlier, the Reynolds number is greater than unity.

Consequently, the flow in the sample of packed spherical beads does not have the characteristics of a purely creeping flow. The Stokes equation (Eq. 8) is therefore not strictly applicable and its use is likely to induce some inaccuracies. However, it seems to us, that Re is not large enough to explain by itself the discrepancy shown in Figures 4 and 5. It should be stressed here that the discrepancy observed between simulated and measured data may also be caused by a packing of the spherical beads within the sample used for the NMR measurements which does not agree with the principles of the reconstruction. This could be addressed using NMR imaging methods to characterize the packing. However, the diameter of the containing tube is about 17 times that of the glass beads; therefore, we do not expect significant edge effects.

Fontainebleau sandstone

Figures 7, 8, and 9 show the normalized average propagators measured in a 25% porosity Fontainebleau sandstone, in absence of flow (Figure 7), in the direction of the flow (Figure 8) and perpendicular to the flow direction (Figure 9). In absence of flow and for the short values of observation times Δ, the shape of the $P_\Delta(X)$ distributions are almost perfectly Gaussian. This arises because the molecules move too short distances for the structure of the Fontainebleau sandstones to have a large influence on the propagators. At longer times, the molecules increasingly encounter the walls. As a result, the effective diffusion constant becomes smaller and the average propagator loses its initial Gaussian behavior to adopt a shape greatly influenced by the structure of the porous media. For displacements measured in the presence of flow, the $P_\Delta(X)$ distributions show an evolution qualitatively similar to the one observed in beads. In particular, from a curve strongly peaked near zero, the distribution obtained in the direction of the flow clearly evolves toward a Gaussian-like shape as the observation time Δ is increased. As reported elsewhere (Packer and Tessier; 1996) for short observation times, the

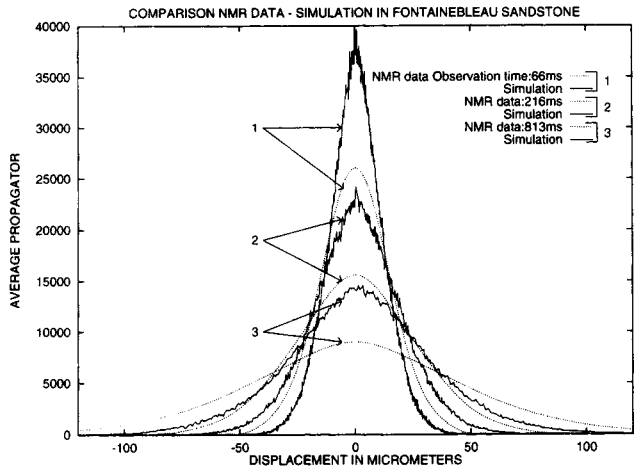

Figure 7. Simulated and measured $P_\Delta(X)$ obtained in absence of flow in a 25% porosity Fontainebleau sandstone.

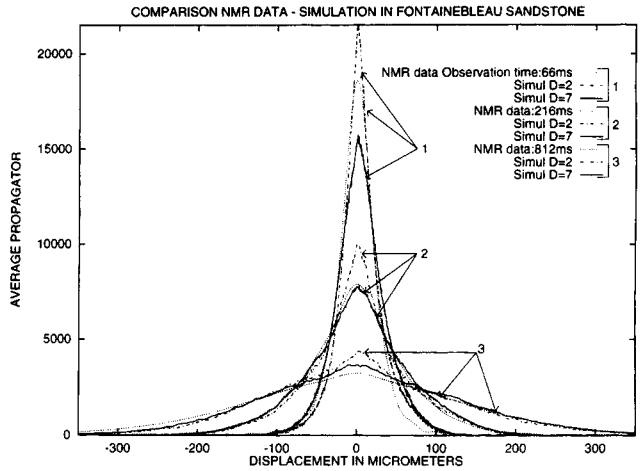

Figure 9. Simulated and measured $P_\Delta(X)$ for brine flow ($Q = 400$ mL/h) in a 25% porosity Fontainebleau sandstone.

Measurements and simulations performed perpendicular to the flow direction. $D = 2$ corresponds to the simulation data obtained with the measured self-diffusion coefficient ($D = 2.1 \times 10^{-9} m^2 \cdot s^{-1}$), while $D = 7$ refers to the simulation performed with the corrected self-diffusion coefficient ($D = 7.245 \times 10^{-9} m^2 \cdot s^{-1}$).

main features of the evolution of the propagators $P_\Delta(X)$ can be explained qualitatively by modeling the porous media as a network of identical capillaries isotropically distributed in terms of their orientation. Assuming laminar flow in each capillary for short observation time, $P_\Delta(X)$ shows a logarithmic discontinuity at zero displacement rounded by the effect of self-diffusion. In order to understand in more detail fluid transport in the Fontainebleau sandstone, a different methodology was used. It is based on the modeling technique described in the previous section and which consists of three majors steps, namely reconstruction, flow, and dispersion. This was applied to a particular sample of Fontainebleau sandstone called GF2 (Adler et al., 1990) as the basis of the reconstruction technique (porosity $\epsilon = 0.251$, correlation length $L = 16.5$ μm). The reconstructed media were made of

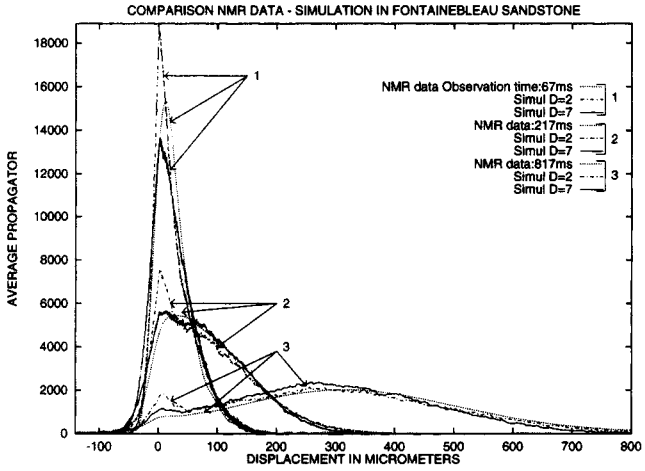

Figure 8. Simulated and measured $P_\Delta(X)$ for brine flow ($Q = 400$ mL/h) in a 25% porosity Fontainebleau sandstone.

Measurements and simulations performed in the direction of the flow. $D = 2$ corresponds to the simulation data obtained with the measured self-diffusion coefficient ($D = 2.1 \times 10^{-9} m^2 \cdot s^{-1}$), while $D = 7$ refers to the simulation performed with the corrected self-diffusion coefficient ($D = 7.245 \times 10^{-9} m^2 \cdot s^{-1}$).

N_C^3 elementary cubes with $N_C = 30$, the elementary cube size is $a = 11.4$ μm, and the total sample size is $N_C \cdot a = 342$ μm. Five samples were generated.

The average interstitial velocity is $\overline{v^*} = 0$ or 372 $\mu m \cdot s^{-1}$, the corresponding Peclet numbers [$Pe = (\overline{v^*} L/D)$] are $Pe = 0$ or 2.92, and these two cases are referred to as $Pe = 0$ and $Pe = 3$.

N^3 grid points were located in each elementary cube ($N = 2$), and the tolerance on the global flux is 10^{-6}.

Additional computations were performed with particle extinction, and particles may disappear at any time or when they hit a solid wall with a probability set so that the global population decays as $e^{-t/\tau}$ with τ of the order of 1.5 s. The results will not be reported here because they did not yield significantly different results.

The sample characteristics are summarized in Table 1. All the samples percolate along the three directions.

The curves representing the experimental and the numerical distributions of the particle displacements are displayed in Figures 8 and 9. The agreement between the NMR experiment and the simulation is encouraging but only semiquantitative.

It is interesting to compare the shapes of the distributions at $Pe = 0$ (Figure 7). A similar propagator is obtained for the NMR data and the simulation, but diffusion seems to be faster in the NMR experiment.

For a Peclet number equal to 3, the details of the distributions along the flow direction is well reproduced in the computations with the existence of two "peaks" in the curves, and the first peak corresponds to diffusion and the second one to convection.

As mentioned earlier, surface extinction did not significantly modify the numerical results.

This first comparison with experiments could be significantly improved in the following way. In porous media, the

Table 1. Sample Characteristics for the Simulated 25% Porosity Fontainebleau Sandstone

Sample	Porosity	Open Porosity	Permeability (mD)			Max. Velocity
			K xx	K xy	K xz	$Vm/\bar{V}^*$
1	0.262	0.253	438	81	4	41.7
2	0.249	0.239	327	27	−17	37.3
3	0.255	0.246	238	−5	−49	40.4
4	0.260	0.254	242	−1	102	49.1
5	0.252	0.244	428	−28	−17	32.7
Avg.	0.256	0.247	335	15	5	40.2

formation factor F is defined as the ratio between the diffusion coefficient D in the free fluid and the rock effective diffusivity coefficient $\bar{D}$

$$F = \frac{D}{\bar{D}} \tag{21}$$

It is known that the formation factor is usually overestimated by the reconstruction technique (Adler et al., 1992), and this is consistent with the observation made in Figure 7 that diffusion is faster in the experiment. This discrepancy can be quantified as follows. In a Gaussian diffusion process, the height $H(t)$ of the central peak of the propagator is related to the constant zeroth-order moment M_o and the second-order moment component along the x-direction M_{xx}^2 as

$$H(t) = \frac{M_o^{3/2}}{\sqrt{2DM_{xx}^2}} \tag{22}$$

It was checked that this integral determination of H is consistent with the peak height actually observed both in simulations and experiments. It is used below, because it is much less noisy than the instantaneous direct value of the propagator for zero displacement.

A least-squares fit of the experimental values of H vs. time in the absence of flow in the time interval 66 to 813 ms yielded

$$H(t) = 8{,}323t^{-0.384} \tag{23}$$

in arbitrary units, with a correlation coefficient $r = 0.9996$. The same fit with the data from the simulations in average over the five reconstructed samples, yielded

$$H(t) = 13{,}360t^{-0.380} \tag{24}$$

with a correlation coefficient $r = 0.996$. The numerical and experimental values of H are plotted vs. time in Figure 10.

Obviously, Eqs. 23 and 24 differ only by a change in time scale with a ratio

$$\left(\frac{8{,}323}{13{,}360}\right)^{-1/0.382} \approx 3.45 \tag{25}$$

This corresponds to an underevaluation of the rock effective diffusivity coefficient by the same factor. This ratio is quite consistent with the overestimation of the numerical predictions of the formation factor of Adler et al. (1992) for Fontainebleau sandstones using the same reconstruction procedure.

The formation factors F of the reconstructed samples were calculated directly by solving the Laplace equation. The average over the five samples was found to be

$$F_{\text{num}} = 37.9 \tag{26}$$

with a standard deviation equal to 10.3. In the meantime, the formation factor of the real rock sample was measured independently by Integrated Core Consultancy Services Ltd. (Middlesex, England) with or without a net hydro-static confining pressure of 200 psi (1.4 MPa). The measurements yielded

$$F_{\text{exp}} = 12.3 \quad (0 \text{ psi})$$

$$F_{\text{exp}} = 10.3 \quad (200 \text{ psi}, 1.4 \text{ MPa})$$

Therefore, the formation factor is numerically overestimated by a factor

$$\frac{F_{\text{num}}}{F_{\text{exp}}} = 3.08 \text{ or } 3.68 \tag{27}$$

This is in good agreement with Eq. 25.

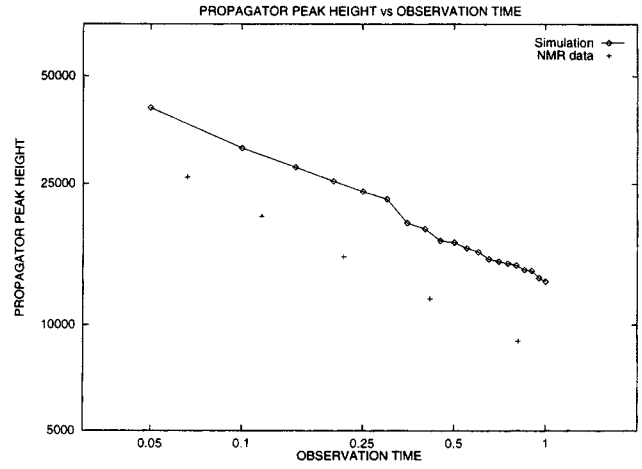

Figure 10. Log-log plot of the central propagator peak height $H(t)$ as a function of time for self-diffusion in a 25% porosity Fontainebleau sandstone.

According to Eq. 21, changing the diffusion coefficient D is actually equivalent to resetting the formation factor. Hence, a new set of numerical simulations was run on the reconstructed sample 1 with a modified molecular diffusion coefficient $D' = 3.45 \times 2.1 \times 10^{-9} = 7.245 \times 10^{-9} m^2/s$ in order to compensate for the overestimated formation factor. Results are presented in Figures 8 and 9 with a flow with mean interstitial velocity $\overline{v^*} = 372$ μm/s, respectively. Clearly, the simulations are greatly improved.

One may therefore conclude that the quantitative departures between the experiments and the random walk simulations result mostly from an underevaluation of the rock effective diffusivity due to the reconstructed samples themselves, and that they may be corrected by resetting the formation factor.

Conclusion

The NMR data acquired both on a sample of packed spherical beads and on a 25% porosity Fontainebleau sandstone illustrate the unique ability of NMR to measure fluid transport within optically opaque porous materials. The NMR protocol used in this study generates the probability distribution $P_\Delta(X)$ of displacement X for different observation times Δ. The propagator $P_\Delta(X)$ thus obtained gives valuable information about the transport of fluids at the pore scale level. We were also able to accurately simulate the transport of an aqueous phase within the rock matrix and generate comparable probability distributions. This result is particularly encouraging since the model applied is based solely upon the structural characteristic of the porous solids.

Acknowledgments

We would like to thank BP Exploration for support for one of us (J.J.T.) as part of BRITE-Euram project EU-5300 and Dr. Kalaydjian (Institut Français du Petrole) for providing the Fontainebleau sandstone.

Literature Cited

Adler, P. M., C. G. Jacquin, and J. A. Quiblier, "Flow in Simulated Porous Media," *Int. J. Multiphase Flow*, **16,** 691 (1990).

Adler, P. M., *Porous Media: Geometry and Transports*, Butterworth/Heinemann, Stoneham, MA (1992).

Adler, P. M., and C. G. Jacquin, and J.-F. Thovert, "The Formation Factor of Reconstructed Porous Media," *Wat. Res. Res.*, **28,** 1571 (1992).

Auzerais, F. M., J. Dunsmuir, B. B. Ferreol, N. Martys, J. Olson, T. S. Ramakraishnan, D. H. Rothman, and L. M. Schwartz, "Transport in Sandstone: A Study Based on Three-Dimensional Microtomography," *Geophys. Res. Lett.*, **23,** 705 (1996).

Callaghan, P. T., *Principles of Nuclear Magnetic Resonance Microscopy*, Clarendon Press, Oxford (1991).

Cenedese, A., and P. Viotti, "Lagrangian Analysis of Nonreactive Pollutant Dispersion in Porous Media by Means of the Particle Image Velocimetry Technique," *Wat. Res. Res.*, **32,** 2329 (1996).

Coelho, D., J.-F. Thovert, and P. M. Adler, "Geometrical and Transport Properties of Random Packings of Spheres and Anisotropic Particles," *Phys. Rev.*, **E55,** 1955 (1997).

Durst, F., A. Melling, and J. H. Whitelaw, *Principles and Practice of Laser-Doppler Anemometry*, 2nd ed., Academic Press, London (1981).

Fordham, E. J., S. G. Gibbs, and L. D. Hall, "Partially Restricted Diffusion in Permeable Sandstone: Observations by Stimulated Echo PFG NMR," *Magn. Reson. Imag.*, **12,** 279 (1994).

Joshi, M., "A Class of Stochastic Models for Porous Media," *PhD, Thesis* Univ. of Kansas, Lawrence (1974).

Kutsovsky, Y., L. Scriven, H. Davis, and B. Hammer, "NMR Imaging of Velocity Profiles and Velocity Distributions in Bead Packs," *Phys. Fluids*, **8,** 863 (1996).

Lebon, L., L. Oger, J. Leblond, J. P. Hulin, N. S. Martis, and L. M. Schwartz, "Pulsed Gradient NMR Measurements and Numerical Simulation of Flow Velocity Distribution in Sphere Packings," *Phys. Fluids*, **8,** 293 (1996).

Lemaitre, R., and P. M. Adler, "Transport in Fractals: IV. Three-Dimensional Stokes flow through Random Media and Regular Fractals," *Transport in Porous Media*, **5,** 325 (1990).

Lucas, A. J., S. G. Gibbs, E. W. Jones, M. Peyron, A. D. Derbyshire, and L. D. Hall, "Diffusion Imaging in the Presence of Static Magnetic Field Gradients," *J. Magn. Reson.* **A-104,** 273 (1993).

Packer, K. J., and J. J. Tessier, "The Characterization of Fluid Transport in a Porous Solid by Pulsed Gradient Stimulated Echo NMR" *Mol. Phys.*, **87,** 267 (1996).

Quiblier, J. A., "A New Three-Dimensional Modeling Technique for Studying Porous Media," *J. Coll. Interf. Sci.*, **98** 84 (1984).

Saleh, S., J.-F. Thovert, and P. M. Adler, "Measurement of Two-Dimensional Velocity Field in Porous Media by Particle Image Displacement Velocimetry Technique," *Wat. Res. Res.*, **32,** 2329 (1996).

Salles, J., J.-F. Thovert, R. Delannay, L. Prevors, J. L. Auriault, and P. M. Adler, "Taylor Dispersion in Porous Media: Determination of the Dispersion Tensor," *Phys. Fluids A*, **5** 2348 (1993).

Spanne, P., J.-F. Thovert, C. J. Jacquin, W. B. Lindquist, K. W. Jones, and P. M. Adler, "Synchrotron Computer Microtomography of Porous Media: Topology and Transports," *Phys. Rev. Lett.*, **73,** 2001 (1994).

Seymour, J. D., and P. T. Callaghan, "Flow-Diffraction, Structural Characterization and Measurement of Hydrodynamic Dispersion in Porous Media by PGSE NMR," *J. Magn. Res.*, **A-122,** 90 (1996).

Manuscript received Oct. 10, 1996, and revision received Feb. 20, 1997.